BRAIN
A JOURNAL OF NEUROLOGY

Diverging longitudinal changes in astrocytosis and amyloid PET in autosomal dominant Alzheimer's disease

Elena Rodriguez-Vieitez,[1] Laure Saint-Aubert,[1] Stephen F. Carter,[1,*] Ove Almkvist,[1,2,3] Karim Farid,[1] Michael Schöll,[1,†] Konstantinos Chiotis,[1] Steinunn Thordardottir,[3,4] Caroline Graff,[3,4] Anders Wall,[5] Bengt Långström[6] and Agneta Nordberg[1,3]

Alzheimer's disease is a multifactorial dementia disorder characterized by early amyloid-β, tau deposition, glial activation and neurodegeneration, where the interrelationships between the different pathophysiological events are not yet well characterized. In this study, longitudinal multitracer positron emission tomography imaging of individuals with autosomal dominant or sporadic Alzheimer's disease was used to quantify the changes in regional distribution of brain astrocytosis (tracer ^{11}C-deuterium-L-deprenyl), fibrillar amyloid-β plaque deposition (^{11}C-Pittsburgh compound B), and glucose metabolism (^{18}F-fluorodeoxyglucose) from early presymptomatic stages over an extended period to clinical symptoms. The 52 baseline participants comprised autosomal dominant Alzheimer's disease mutation carriers ($n = 11$; 49.6 ± 10.3 years old) and non-carriers ($n = 16$; 51.1 ± 14.2 years old; 10 male), and patients with sporadic mild cognitive impairment ($n = 17$; 61.9 ± 6.4 years old; nine male) and sporadic Alzheimer's disease ($n = 8$; 63.0 ± 6.5 years old; five male); for confidentiality reasons, the gender of mutation carriers is not revealed. The autosomal dominant Alzheimer's disease participants belonged to families with known mutations in either presenilin 1 (*PSEN1*) or amyloid precursor protein (*APPswe* or *APParc*) genes. Sporadic mild cognitive impairment patients were further divided into ^{11}C-Pittsburgh compound B-positive ($n = 13$; 62.0 ± 6.4; seven male) and ^{11}C-Pittsburgh compound B-negative ($n = 4$; 61.8 ± 7.5 years old; two male) groups using a neocortical standardized uptake value ratio cut-off value of 1.41, which was calculated with respect to the cerebellar grey matter. All baseline participants underwent multitracer positron emission tomography scans, cerebrospinal fluid biomarker analysis and neuropsychological assessment. Twenty-six of the participants underwent clinical and imaging follow-up examinations after 2.8 ± 0.6 years. By using linear mixed-effects models, fibrillar amyloid-β plaque deposition was first observed in the striatum of presymptomatic autosomal dominant Alzheimer's disease carriers from 17 years before expected symptom onset; at about the same time, astrocytosis was significantly elevated and then steadily declined. Diverging from the astrocytosis pattern, amyloid-β plaque deposition increased with disease progression. Glucose metabolism steadily declined from 10 years after initial amyloid-β plaque deposition. Patients with sporadic mild cognitive impairment who were ^{11}C-Pittsburgh compound B-positive at baseline showed increasing amyloid-β plaque deposition and decreasing glucose metabolism but, in contrast to autosomal dominant Alzheimer's disease carriers, there was no significant longitudinal decline in astrocytosis over time. The prominent initially high and then declining astrocytosis in autosomal dominant Alzheimer's disease carriers, contrasting with the increasing amyloid-β plaque load during disease progression, suggests astrocyte activation is implicated in the early stages of Alzheimer's disease pathology.

1 Department NVS, Centre for Alzheimer Research, Division of Translational Alzheimer Neurobiology, Karolinska Institutet, 141 57 Huddinge, Stockholm, Sweden
2 Department of Psychology, Stockholm University, 106 91 Stockholm, Sweden
3 Department of Geriatric Medicine, Karolinska University Hospital Huddinge, 141 86, Stockholm, Sweden
4 Department NVS, Center for Alzheimer Research, Division of Neurogeriatrics, Karolinska Institutet, 141 57 Huddinge, Stockholm, Sweden
5 Department of Surgical Sciences, Section of Nuclear Medicine & PET, Uppsala University, 751 85 Uppsala, Sweden

6 Department of Chemistry, Uppsala University, 701 05 Uppsala, Sweden

*Present address: Wolfson Molecular Imaging Centre, University of Manchester, Manchester, M20 3LJ, UK
†Present address: MedTech West and the Department of Clinical Neuroscience and Rehabilitation, University of Gothenburg, 413 45 Gothenburg, Sweden

Correspondence to: Agneta Nordberg, MD, PhD, Professor,
Karolinska Institutet, Department of Neurobiology, Care Sciences and Society,
Division of Translational Alzheimer Neurobiology,
Novum 5th Floor, Blickagången 6, SE-141 57 Huddinge,
Sweden
E-mail: Agneta.K.Nordberg@ki.se

Introduction

Alzheimer's disease is a multifactorial dementia disorder with a long preclinical phase characterized by a cascade of pathophysiological events (Braak and Braak, 1991; Holtzman *et al.*, 2011; Zlokovic, 2011; Heneka *et al.*, 2015*a*). The study of autosomal dominant Alzheimer's disease (ADAD), caused by mutations in the presenilin 1 (*PSEN1*), presenilin 2 (*PSEN2*) and amyloid precursor protein (*APP*) genes, has allowed the age of symptom onset for a specific mutation to be predicted and facilitates investigation of the evolution of pathology in ADAD from presymptomatic stages. The value of ADAD as a model for predicting the time course of neuropathological changes in the much more common and complex sporadic Alzheimer's disease forms remains under discussion (Bateman *et al.*, 2011; Fleisher, 2014). A recent cross-sectional study found similarities in functional connectivity as related to cognitive symptoms between ADAD and sporadic Alzheimer's disease (Thomas *et al.*, 2014); however, to our knowledge no previous study has yet compared the longitudinal progression of *in vivo* biomarkers in ADAD versus sporadic Alzheimer's disease. Recent PET imaging studies of ADAD (Bateman *et al.*, 2012; Fleisher *et al.*, 2012, 2015; Benzinger *et al.*, 2013; Fleisher *et al.*, 2015) and sporadic Alzheimer's disease (Villemagne *et al.*, 2013) have shown that the earliest observed pathological changes related to amyloid-β plaque deposition can be measured 15 to 20 years before the onset of clinical symptoms, and that changes in glucose metabolism develop later in the presymptomatic stages (Schöll *et al.*, 2011*a*; Benzinger *et al.*, 2013). The various findings on the evolution of biomarkers in Alzheimer's disease have contributed to the establishment of models of the temporal evolution of amyloid-β and tau deposition, metabolism and atrophy (Jack and Holtzman, 2013), the increased incorporation of biomarkers in the diagnosis of Alzheimer's disease (Dubois *et al.*, 2014), and the inclusion of biomarkers as endpoints in clinical trials of new therapeutic agents.

Nonetheless, there is increasing evidence that pathological processes independent of amyloid-β plaque deposition may contribute to the initiation of Alzheimer's disease (Hyman, 2011; Chételat, 2013). Glial activation and neuroinflammation are increasingly recognized as early events in the disease, even preceding amyloid-β plaque deposition (Heneka *et al.*, 2015*a, b*), potentially making glia a promising therapeutic target (Barres, 2008; Fuller *et al.*, 2009; Thal, 2012). Astrocytes, the most numerous brain cell type, can be classified into a diversity of subpopulations (Zhang and Barres, 2010; Oberheim *et al.*, 2012). Activated astrocytes, which have been investigated most often in post-mortem neuropathological studies, have wide phenotypic heterogeneity (atrophic/hypertrophic) (Barres, 2008; Anderson *et al.*, 2014); astrocytic markers, including glial fibrillary acidic protein (GFAP), glutamine synthetase, vimentin, nestin (measured by immunohistochemistry), and monoamine oxidase-B (MAOB) [primarily located in activated astrocytes (Ekblom *et al.*, 1993; Saura *et al.*, 1994) and measured by ^{3}H-L-deprenyl autoradiography (Verkhratsky *et al.*, 2015)], display varying levels of expression.

Post-mortem analyses of astrocytosis in human Alzheimer's disease brain tissue have reported conflicting findings. While GFAP-positive activated astrocytes have been found next to fibrillar amyloid-β plaques in some studies (Yu *et al.*, 2005; Gulyás *et al.*, 2011), others (Kadir *et al.*, 2011; Marutle *et al.*, 2013) found no regional correlations between activated astrocytes as measured by ^{3}H-L-deprenyl (MAOB tracer) and fibrillar amyloid-β plaques measured by ^{3}H-Pittsburgh compound B. These results suggest that activated astrocytes assessed using GFAP may be different or have a different type of activation from those assessed using ^{3}H-L-deprenyl, depending on the stage of disease progression. Astrocyte activation, including the overexpression of MAOB, is associated with the release of reactive oxygen species, potentially leading

Table 1 Demographic and clinical information

	ADAD-family participants			Patients with sporadic Alzheimer's disease		
	Non-carrier	pMC	sMC	PiB- MCI	PiB+ MCI	Alzheimer's disease
n at baseline (total = 52)	16	7	4[a]	4	13	8
Gender	10M/6F	[b]	2M/2F	2M/2F	7M/6F	5M/3F
Estimated years to symptom onset	−4.4 ± 12.6	−10.1 ± 9.1	0.8 ± 3.3			
Baseline age, years	51.1 ± 14.2	44.9 ± 9.8	58.0 ± 3.7	61.8 ± 7.5	62.0 ± 6.4	63.0 ± 6.5
Education, years	11.1 ± 2.0	12.1 ± 2.0	9.8 ± 1.0	13.8 ± 2.2	13.7 ± 2.3	11.0 ± 2.3
APOE4 + (%)	5 (31)	3 (43)	2 (50)	1 (25)	10 (77)	6 (75)
CSF amyloid-β_{42}, pg/ml	N/A	N/A	302 ± 130	1160 ± 203	537 ± 148	506 ± 158
CSF total-tau, pg/ml	N/A	N/A	723 ± 302	257 ± 46	404 ± 152	608 ± 321
CSF phospho-tau, pg/ml	N/A	N/A	110 ± 23	55 ± 20	67 ± 16	93 ± 30
MMSE at baseline	28.9 ± 1.2	29.6 ± 0.5	16.0 ± 8.7	27.3 ± 2.1	27.8 ± 1.8	23.8 ± 5.7
Global cognition at baseline (z-score)	0.13 ± 0.66	0.49 ± 0.55	**−3.10 ± 4.53**	− 0.31 ± 0.80	− 0.73 ± 1.0	**−2.06 ± 2.04**
Episodic memory at baseline (z-score)	−0.11 ± 0.48	−0.06 ± 0.49	**−2.15 ± 0.89**	**−1.20 ± 0.91**	**−1.36 ± 0.72**	**−2.25 ± 0.72**
n at follow-up (total = 26)	8	7[c]	1	2	6[d]	2
Follow-up time, years	3.0 ± 0.5	2.7 ± 0.2	2.8	3.8 ± 0.1	2.3 ± 0.7	3.4 ± 0.7

Data are presented as means ± SD except when the group had fewer than three participants (in which case the individual values are displayed). Normal CSF values: amyloid-β_{42} > 550 pg/ml, total-tau < 400 pg/ml, phospho-tau < 60 pg/ml. The average follow-up time for all groups was 2.8 ± 0.6 years. All neuropsychology values are mean z-scores ± SD; z-scores below −1.645 were considered outside the range of healthy individuals from an age-matched healthy population. Neuropsychology values in bold were considered outside the normal range.
[a]Two were diagnosed with MCI and two with Alzheimer's disease. One of the MCI patients was followed up (MCI diagnosis retained).
[b]Gender distribution of presymptomatic mutation carriers is not revealed to preserve confidentiality.
[c]One had developed MCI at follow-up.
[d]Three had converted to Alzheimer's disease at follow-up and three remained as PiB + MCI.
F = female; M = male; MMSE = Mini-Mental State Examination; N/A = not available.

to excessive oxidative damage, neuroinflammatory changes, more amyloid-β plaque deposition, and other pathological changes in Alzheimer's disease (Miller, 2005). These studies demonstrate the complexity of the functions of activated astrocytes; little is known about their *in vivo* relationships with other disease biomarkers. While there is an increasing interest in the *in vivo* molecular imaging of glial activation and neuroinflammation, most studies have focused on activated microglia (Jacobs *et al.*, 2012; Zimmer *et al.*, 2014; Varley *et al.*, 2015).

The PET tracer ^{11}C-deuterium-L-deprenyl (^{11}C-DED) binds specifically to MAOB (Fowler *et al.*, 1987, 2005) and has been applied to investigate astrocytosis in neurodegenerative diseases including Alzheimer's disease (Johansson *et al.*, 2007; Santillo *et al.*, 2011). Significantly increased ^{11}C-DED binding was found in prodromal stages of Alzheimer's disease in comparison to healthy controls or to patients with Alzheimer's disease dementia (Carter *et al.*, 2012). Additionally, ^{11}C-DED PET binding was negatively correlated with grey matter density in prodromal Alzheimer's disease (Choo *et al.*, 2014). These findings indicate that further investigation of the early progressive brain changes in both the autosomal dominant and sporadic forms of the disease is warranted. The aim of this multitracer PET imaging study was to investigate in detail the comparative regional and temporal patterns of *in vivo* brain astrocytosis, fibrillar amyloid-β deposition, and glucose metabolism in patients with ADAD or sporadic Alzheimer's disease.

Materials and methods

Study design and participants

Individuals from families with known ADAD mutations were recruited along with sporadic patients referred for memory problems to the Department of Geriatric Medicine, Karolinska University Hospital Huddinge (Stockholm, Sweden). A total of 52 participants were included at baseline, and 26 of these were followed-up 2.8 ± 0.6 years after baseline (Table 1). This study is a continuation of a cross-sectional multivariate analysis study performed on a subset of participants at baseline (Schöll *et al.*, 2015). All participants underwent a comprehensive clinical and imaging examination at baseline and follow-up, including medical history, neurological and psychiatric examination, electroencephalography, MRI, CSF, apolipoprotein E (*APOE*) genotyping from blood sample, and neuropsychological assessment. Details on the CSF and neuropsychological assessment methods are included in the Supplementary materials.

The diagnosis of mild cognitive impairment (MCI) followed the criteria by Petersen (2004), and Alzheimer's disease dementia was diagnosed according to the criteria of the National Institute of Neurological and Communicative Disorders and Stroke, and the Alzheimer's Disease and Related Disorders Association (NINCDS-ADRDA) (McKhann *et al.*, 1984). Diagnoses were made during a consensus meeting where a geriatrician/neurologist, a neuropsychologist and a nurse discussed the outcome of the assessment of the patients. All participants provided written informed consent to participate in the study, which was

conducted according to the Declaration of Helsinki and subsequent revisions. Ethical approval was obtained from the regional Human Ethics Committee of Stockholm and the Faculty of Medicine and Radiation Hazard Ethics Committee of Uppsala University Hospital, Sweden.

Autosomal dominant Alzheimer's disease family members

The ADAD participants in this study are part of an ongoing research study at Karolinska Institutet involving families carrying one of four mutation types, each with a different average age of onset. For a given participant, the age of symptom onset is defined as the age at which the first clinically relevant cognitive symptoms appear, either as experienced by the patient or by near relatives. The *PSEN1* Ile143Thr mutation (Keller *et al.*, 2010) has the earliest average age of symptom onset at 36 ± 2 years, while the other three mutations have similar average age of symptom onset: *PSEN1* His163Tyr at 52 ± 7 years, *APP*swe KM670/671NL at 54 ± 5 years, and *APP*arc Glu693Gly at 56 ± 3 years (Thordardottir *et al.*, 2014). These values were estimated as averages based on the medical records of individuals from each of the families (five, nine, 24 and 12 individuals for the four mutation types, respectively). This method of estimating average age of symptom onset has been validated by a recent meta-analysis (Ryman *et al.*, 2014). Participants in our study were non-carriers, presymptomatic mutation carriers (pMC), or symptomatic mutation carriers (sMC). sMC patients were either clinically diagnosed as having MCI (Petersen, 2004) or Alzheimer's disease dementia (McKhann *et al.*, 1984), and are receiving medication. Individuals from the pMC group had no cognitive complaints and did not fulfil the criteria for MCI or Alzheimer's disease dementia. To preserve confidentiality, individual mutation statuses are not provided. All clinicians and researchers in contact with and examining the ADAD-family members as well as the research subjects were blind to the mutation status.

Subjects with sporadic Alzheimer's disease

Patients in the sporadic group either had MCI (Petersen, 2004) or probable Alzheimer's disease dementia (McKhann *et al.*, 1984). MCI patients were further divided into Pittsburgh compound B (PiB)-positive (PiB+) and PiB-negative (PiB−) groups using a cut-off value of 1.41 neocortical standardized uptake value ratio (SUVR) with reference to the cerebellar grey matter, as previously described (Nordberg *et al.*, 2013). The subgroup of PiB+ MCI patients fulfils the current diagnostic criteria for prodromal Alzheimer's disease (Dubois *et al.*, 2014).

Healthy control subject recruitment

Two control groups were used in this study. A group of 14 healthy control subjects with a mean age of 64.7 ± 3.6 years and no family history of Alzheimer's disease underwent MRI and ^{11}C-DED PET imaging alone. This group was obtained from a previously published study (Carter *et al.*, 2012), which provides further information about recruitment details. The group of 14 healthy subjects was used as control group for

^{11}C-DED binding. A second control group composed of the ADAD-family non-carrier subjects ($n = 16$) was used as control for ^{11}C-PiB retention and ^{18}F-fluorodeoxyglucose (^{18}F-FDG) uptake. For simplicity, we have referred to both groups as Control groups throughout this study.

PET and MRI image acquisition and processing

Participants underwent PET examinations with ^{11}C-DED, ^{11}C-PiB, and ^{18}F-FDG at the Uppsala PET Centre, Uppsala University (Sweden) on ECAT EXACT HR+ (Siemens/CTI) and GE discovery ST PET/CT scanners. The tracers were produced and the PET and MRI image acquisition and processing methods were set as previously described (Carter *et al.*, 2012); further details are included in the Supplementary material. Briefly, for each participant, a T_1 MRI image was acquired at baseline and co-registered onto the individual's ^{11}C-DED late-sum (10–60 min) image in native ^{11}C-DED space using SPM8; ^{11}C-PiB and ^{18}F-FDG late-sum images (40–60 and 30–45 min, respectively) were co-registered onto the T_1 MRI image (which had been previously co-registered to native ^{11}C-DED space). This T_1 MRI image was segmented and a binary grey matter mask was created from the resultant probabilistic grey matter map (threshold = 0.5). Using the inverse non-linear transformation from this segmentation, a simplified probabilistic atlas (Hammers *et al.*, 2003) consisting of 12 bilateral regions of interest was registered from the MNI (Montreal Neurological Institute) space back into the subject's native ^{11}C-DED space, and masked using the individual binary grey matter mask. Registered ^{18}F-FDG and ^{11}C-PiB PET images for each participant were sampled using the created individual cortical atlas; the whole pons was used as a reference as it was found to be preserved from pathology in both ADAD and sporadic Alzheimer's disease (Minoshima *et al.*, 1995). For ^{11}C-DED quantification, a modified reference Patlak model (Johansson *et al.*, 2007) was applied to the 20–60 min dynamic ^{11}C-DED PET images using the cerebellar grey matter as the modified reference region (Gulyás *et al.*, 2011) to generate individual 3D parametric Patlak slope images (units: min^{-1}). The model assumed a cerebellar grey matter slope value of 0.01 min^{-1}. ^{11}C-DED binding was then expressed as the ratio of the ^{11}C-DED slope value in the target region of interest to that in the cerebellar grey matter, as previously reported (Johansson *et al.*, 2007). This processing was applied to baseline and follow-up PET images.

Statistical analysis

Group comparisons of all variables were performed using two-tailed Kruskal-Wallis tests, followed by *post hoc* Mann-Whitney non-parametric pair-wise comparisons. The Mann-Whitney effect size was calculated using $r = z/(\sqrt{N})$, where z is the Mann-Whitney z-score and N the sum of individuals from the two groups being compared. All group comparisons were performed, separately for 12 regions of interest, and across four diagnostic groups: pMC, Control group, PiB+ MCI and sporadic Alzheimer's disease groups. A multiple comparisons

procedure controlling for false discovery rate as implemented in the Benjamini-Hochberg method (Benjamini and Hochberg, 1995) using pplot software (Turkheimer et al., 2001) was applied to correct for multiple regional tests. The post hoc pair-wise Mann-Whitney comparisons were further corrected for multiple comparisons using the Dunn-Bonferroni method (Dunn, 1964). Among the seven pMC subjects, one was an APParc carrier and thus had low ^{11}C-PiB retention (Schöll et al., 2012), and was removed from statistical analyses of ^{11}C-PiB PET. Another pMC subject had passed the age of onset, and showed no penetrance of the mutation, and hence this subject was removed from all statistical analyses. Pair-wise associations between regional ^{11}C-PiB, ^{11}C-DED and ^{18}F-FDG within diagnostic groups were tested using Spearman's correlation (r_S). Significance level was set at $P < 0.05$; a multiple comparisons procedure controlling for false discovery rate as implemented in the Benjamini-Hochberg method (Benjamini and Hochberg, 1995) using pplot software (Turkheimer et al., 2001) was applied to correct for multiple regional tests. The above analyses were performed using SPSS (IBM SPSS Statistics, Version 22.0), unless otherwise noted.

Voxel-wise PET group comparisons were performed using the SPM8 two-sample t-test model. A threshold was set at $P = 0.001$ (uncorrected); for this threshold, clusters greater than 20 voxels were considered significant.

The estimated years to symptom onset was calculated for both carriers and non-carrier participants by subtracting each participant's age from the average age of symptom onset for the corresponding mutation type in the respective family. To assess regional differences in the longitudinal trajectories of PET retention in mutation carriers and non-carrier subjects, PET tracer retention was modelled separately for each region of interest using a linear mixed-effects model (LMM) implemented in the non-linear mixed-effects (NLME) package in R (version 3.0.1, The R Foundation for Statistical Computing, http://www.r-project.org/). The model incorporated estimated years to symptom onset as a linear fixed-effect variable, and a random intercept at the subject level to account for longitudinal within-individual correlations. The restricted maximum likelihood estimation option was used to fit all models. The time point at which the longitudinal trajectories of mutation carriers versus non-carriers started to diverge was conservatively determined as the estimated years to symptom onset after which the two 95% confidence bands no longer overlapped. An LMM (NLME package in R) was also applied to assess the longitudinal evolution of regional PET tracer retention in sporadic PiB+ MCI patients using a fixed effect for time (number of years since MCI clinical diagnosis) and a random intercept at the subject level. The significance level for all model intercept and slope values was set at $P < 0.05$. In addition, a multiple comparisons procedure controlling for false discovery rate as implemented in the Benjamini-Hochberg method (Benjamini and Hochberg, 1995) using pplot

software (Turkheimer et al., 2001) was applied to correct for multiple regional tests.

Results

Demographic and clinical information on the participants is provided in Table 1. All groups were matched for age, except for the pMC group, which was significantly younger than the sporadic patient groups ($P = 0.001$ versus PiB+ MCI, and $P = 0.005$ versus Alzheimer's disease). The Alzheimer's disease and sMC groups showed significant impairment ($z < -1.645$) in both global cognition and episodic memory. In addition, the PiB+ MCI group had poor episodic memory performance, as measured by a z-score of -1.36 (SD 0.72), close to the threshold of abnormality.

Neuropsychological profiles at baseline and follow-up

Global cognition and episodic memory performance remained stable in the pMC, non-carrier, and PiB− MCI groups from baseline to follow-up examination. The only sMC subject who was retested at follow-up showed somewhat declining performance in both global cognition (from z = 0.06 to −0.94) and episodic memory (from z = −1.21 to −1.33). The episodic memory performance of the PiB+ MCI group was significantly worse at follow-up than at baseline, decreasing from z = −1.36 (SD 0.72; n = 13) to −2.16 (SD 0.93; n = 6; $P = 0.046$ versus baseline, Wilcoxon non-parametric paired t-test). The two Alzheimer's disease patients who received follow-up examinations showed reduced global cognition (from z = −0.94 to −2.75 and from z = −0.67 to −3.59, respectively) and poorer episodic memory (from z = −1.89 to −2.37 and from z = −1.91 to −3.06, respectively).

Baseline profiles of ^{11}C-PiB, ^{11}C-DED and ^{18}F-FDG retention in autosomal dominant and sporadic Alzheimer's disease

The cross-sectional comparison of regional PET retention data between the different diagnostic groups with ^{11}C-PiB, ^{11}C-DED and ^{18}F-FDG markers is illustrated in Fig. 1 for five selected regions of interest; mean retention values are given in Supplementary Table 1. All statistical comparisons across the groups (pMC, PiB+ MCI, Alzheimer's disease and Control groups) are presented in Supplementary Table 2, where the pMC group is composed of those presymptomatic mutation carriers whose age was lower than the average age of symptom onset. A sensitivity study including an additional individual in the pMC group who was older than the average age of symptom onset demonstrated that the statistical comparisons remained significant whether this individual was included or not (Supplementary Table 3).
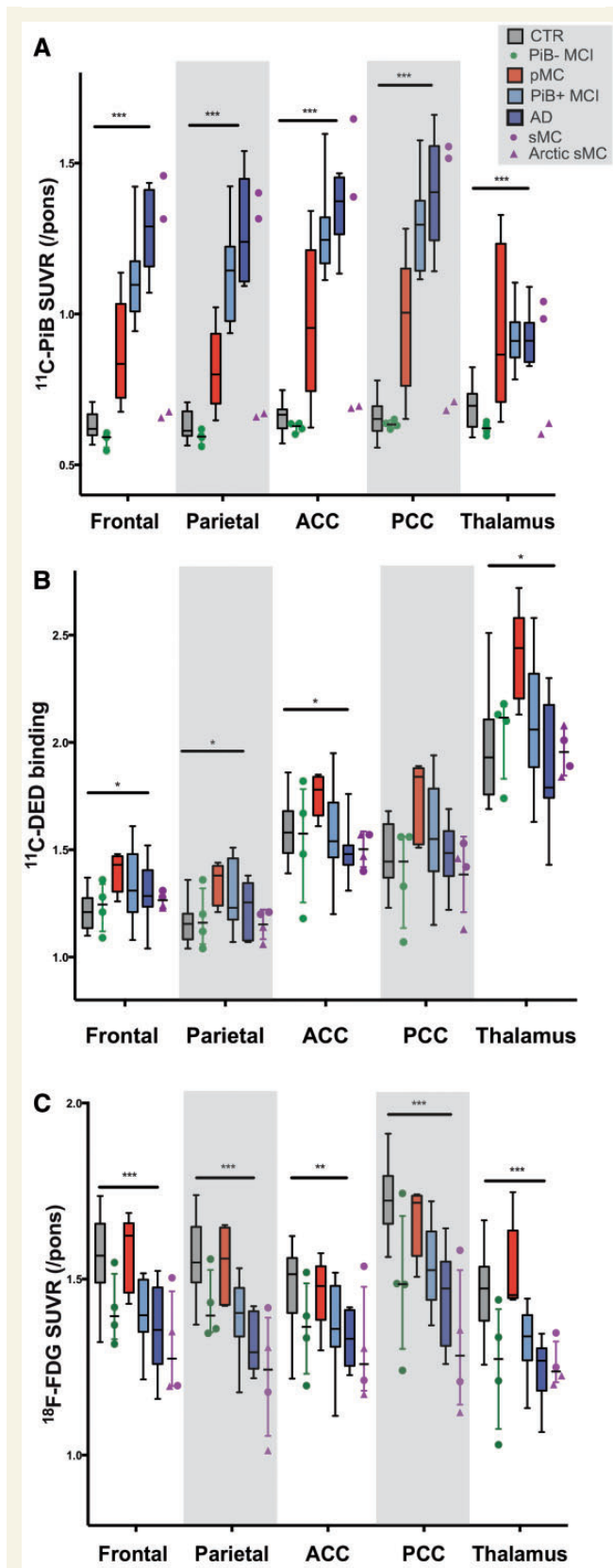
Figure 1 Cross-sectional PET retention data. Cross-sectional PET retention data for all diagnostic groups at baseline, represented as boxplots (except for groups with *n* ⩽ 4, which are represented by scatter dot plots), are shown for five selected bilateral regions of interest: frontal, parietal, ACC, PCC, and thalamus

The ^{11}C-PiB retention values differed significantly across the groups (pMC, PiB+ MCI, Alzheimer's disease and Control group) in all regions of interest except in the hippocampus, and they remained significant after correction for multiple comparisons (Fig. 1A and Supplementary Table 2). In *post hoc* pair-wise comparisons, ^{11}C-PiB retention was significantly higher in the pMC group than in the Control group for all regions of interest except the parahippocampus, with the largest effect sizes in the frontal (r = 0.67, P = 0.003) and temporal (r = 0.63, P = 0.005) regions. In contrast, ^{11}C-PiB retention was significantly lower in the pMC group than in PiB+ MCI patients for all regions of interest except subcortical regions. Both PiB+ MCI and Alzheimer's disease groups had significantly higher ^{11}C-PiB retention than the Control group, with large effects sizes in all regions (r > 0.80). Figure 1A also shows some degree of variability of ^{11}C-PiB retention in pMC carriers and, in particular, the typical ^{11}C-PiB-negative profile of Arctic mutation carriers in all regions.

Comparison of ^{11}C-DED binding across the subject groups (pMC, PiB+ MCI, Alzheimer's disease and Control group) showed statistically significant differences in four regions of interest at the group level: frontal (P = 0.037), parietal (P = 0.014), anterior cingulate cortex (P = 0.036) and thalamus (P = 0.017) (Fig. 1B and Supplementary Table 2); statistical results in the parietal lobe and the thalamus remained significant after multiple-comparisons correction. *Post hoc* pair-wise statistical comparisons showed that the pMC group had higher ^{11}C-DED binding (astrocyte activation) than any other group. The effect sizes were largest for the comparison between pMC and Alzheimer's disease patients, in particular in the anterior cingulate cortex (r = 0.73, P = 0.008) and thalamus (r = 0.69, P = 0.013). ^{11}C-DED binding was also higher in the pMC than in the Control group, with large effect sizes in the frontal (r = 0.64, P = 0.005), parietal (r = 0.66, P = 0.004), thalamus (r = 0.55, P = 0.016) and anterior cingulate cortex (r = 0.51, P = 0.026) regions. ^{11}C-DED binding was also significantly higher in the pMC group than in

for (**A**) ^{11}C-PiB SUVR with reference to the pons, (**B**) ^{11}C-DED binding given by the ratio of the Patlak slope in the region in min^{-1} to that in the cerebellar grey matter ($0.01\,min^{-1}$), and (**C**) ^{18}F-FDG SUVR with reference to the pons. The pMC group consisted of the five subjects who were younger than the average age of onset. Two symptomatic Arctic mutation carriers are represented by separate symbols (triangles), as subjects with this mutation have very low ^{11}C-PiB retention. Groups represented are pMC (*n* = 5), sMC (*n* = 4), PiB − MCI (*n* = 4), PiB + MCI (*n* = 13), sporadic Alzheimer's disease (*n* = 8), and the Control group, composed of non-carrier members of ADAD families (*n* = 16) for ^{11}C-PiB and ^{18}F-FDG PET, and healthy subjects (*n* = 14) for ^{11}C-DED PET. Horizontal bars over boxplots indicate that differences in PET retention were significant at group level (pMC, PiB + MCI, sporadic Alzheimer's disease, Control group); *P < 0.05, **P < 0.01, ***P < 0.001. ACC = anterior cingulate cortex; AD = Alzheimer's disease; CTR = control; MCI = sporadic mild cognitive impairment; PCC = posterior cingulate cortex; ROI = region of interest.

PiB+ MCI patients in the thalamus (r = 0.50, P = 0.034) and tended to be higher in the anterior cingulate cortex (r = 0.043, P = 0.068).

In patients with sporadic disease, ^{11}C-DED binding was significantly higher in the PiB+ MCI group than in the Control group in the parietal region (r = 0.46, P = 0.017) and tended to be higher in the frontal cortex (r = 0.35, P = 0.073). There was also a trend for higher ^{11}C-DED binding in the PiB + MCI group than in the Alzheimer's disease group in the thalamus (r = 0.38, P = 0.082). ^{11}C-DED binding in the Alzheimer's disease group was not statistically different from that in the Control group, except for a trend for higher binding in the frontal region (r = 0.39, P = 0.065).

For ^{18}F-FDG uptake (Fig. 1C), all regions of interest were statistically significant at the group level (Supplementary Table 2); results in all regions of interest except for the putamen remained significant after multiple-comparisons correction. The pMC and Control groups had significantly higher ^{18}F-FDG uptake in most brain regions than seen in either PiB+ MCI or Alzheimer's disease patients. There were no significant differences in ^{18}F-FDG uptake between the pMC and Control group, or between the PiB+ MCI and Alzheimer's disease patients, in any region of interest.

The correlations between the three tracers were assessed within each group for the 12 regions of interest. In the sporadic PiB+ MCI group, a significant positive correlation was found between ^{11}C-PiB retention and ^{11}C-DED binding values in the frontal lobe (r_s = 0.57, P = 0.042), which did not survive correction for multiple comparisons. No significant correlations were found between ^{11}C-PiB and ^{11}C-DED in the Alzheimer's disease, pMC or Control groups. Nor were significant correlations found between ^{18}F-FDG and ^{11}C-PiB, or ^{18}F-FDG and ^{11}C-DED in the pMC, PiB+ MCI, Alzheimer's disease or Control groups.

Presymptomatic mutation carrier PET imaging profiles at baseline and follow-up using voxel-wise analysis

The individual PET imaging profiles for the three tracers are shown for the five pMC participants who were younger than the expected age of onset and for the only followed sMC patient in Fig. 2A, while whole brain comparisons for the pMC versus Control groups, and the pMC versus PiB+ MCI groups, are shown in Fig. 2B (statistical results are shown in Supplementary Table 4). On ^{11}C-PiB PET imaging, retention was significantly higher in the pMC group than in the Control group at baseline, predominantly in the frontal lobe and the insula bilaterally, but also in all other lobes in the right hemisphere and in the right thalamus. Similar results were observed at follow-up, with greater extent. Contrariwise, the pMC group had significantly lower ^{11}C-PiB retention than the PiB+ MCI group at baseline in the right temporal and bilateral frontal lobes, as well as in the left anterior cingulate cortex, although the

comparison did not reach significance at the cluster level. Significantly lower ^{11}C-PiB retention was also found at follow-up, involving the bilateral frontal, temporal and parietal regions.

The binding of ^{11}C-DED PET was significantly higher at baseline in the pMC than in the Control group in the parietal regions (inferiolateral region, postcentral gyrus), the posterior cingulate cortex, the right frontal regions (anterior cingulate cortex, precentral gyrus), the left occipital regions, and the bilateral thalamus. At follow-up, binding remained higher in the pMC group in the fronto-parietal regions, including additional frontal regions. The pMC subjects also had significantly higher ^{11}C-DED binding at baseline than the PiB+ MCI patients in the anterior cingulate cortex and the right thalamus, as well as in temporal clusters. Clusters in the temporal lobe also had significantly higher binding at the peak level. At follow-up, the significant regions were distributed across other frontal regions as well as the left thalamus.

Glucose metabolism as measured by ^{18}F-FDG PET uptake was lower in the left parietal region at baseline in the pMC group than in the Control group, with significance reached at the peak level only (postcentral gyrus, superior parietal gyrus). This difference spread to the left posterior cingulate cortex and other parietal regions (remainder of the left inferiolateral region, bilateral superior parietal gyrus) and to the left middle frontal gyrus and the bilateral cuneus at follow-up. When compared to sporadic PiB+ MCI patients, the pMC group had higher ^{18}F-FDG uptake at baseline in the frontal and temporal regions, and in the right thalamus. Similar results were found at follow-up.

Of note, none of the opposite contrasts showed significant clusters in any of the mentioned comparisons, for any of the three PET tracers.

Longitudinal trajectories of regional ^{11}C-PiB, ^{11}C-DED and ^{18}F-FDG PET retention in autosomal dominant Alzheimer's disease

A LMM was used to estimate the temporal evolution of PET tracer retention in the ADAD group (including both pMC and sMC groups) and the non-carrier group in the different regions of interest (Figs 3–5) with respect to estimated years to symptom onset, resulting in positive rates of change in ^{11}C-PiB retention and negative rates of change in both ^{11}C-DED binding and ^{18}F-FDG uptake in mutation carriers, which remained significant in the majority of regions of interest after multiple-comparisons correction. There was no statistically significant change in the non-carrier group for ^{11}C-PiB retention or ^{11}C-DED binding. ^{18}F-FDG significantly declined with age in the non-carrier group in selected regions, but the decline was not significant after multiple-comparisons correction. Table 2 includes all significant regional rates of change in PET
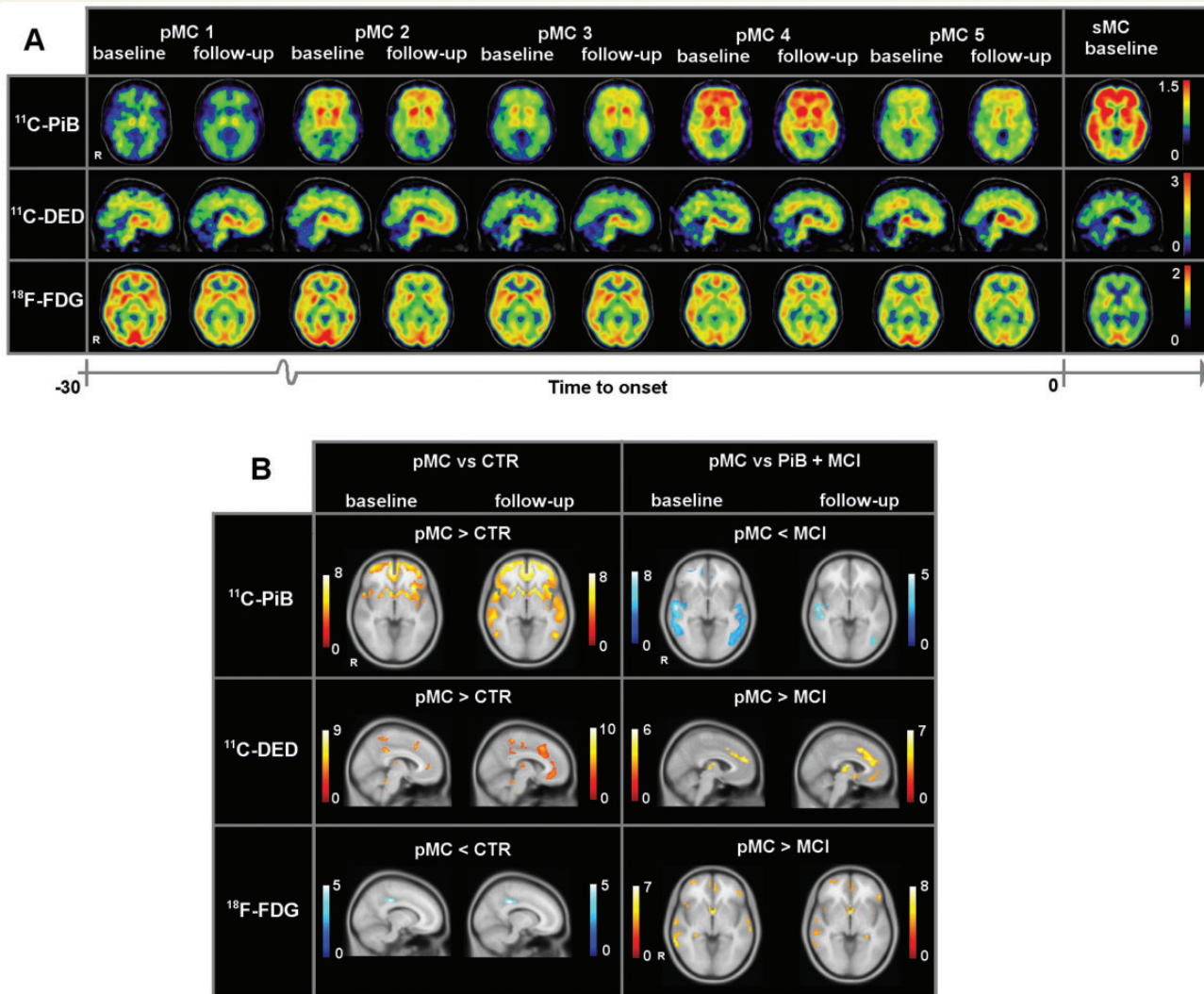
Figure 2 Presymptomatic mutation carriers: individual profiles and voxel-wise inter-group comparisons. (**A**) Individual retention of ^{11}C-PiB (axial section; SUVR), ^{11}C-DED (sagittal section; Patlak slope), and ^{18}F-FDG (axial section; SUVR) in five evaluable pMC individuals at baseline and follow-up, and in one sMC patient at baseline. (**B**) Voxel-wise inter-group comparison (using SPM8) for each tracer between the five pMC participants at baseline and follow-up and the Control group (*left*) and sporadic PiB + MCI group (*right*) at baseline only. Statistical threshold: $P < 0.001$ (uncorrected). Cluster size $\geqslant 20$ voxels. The red and yellow scales correspond to contrasts showing higher retention in the pMC group, and the blue scales correspond to those showing lower retention in the pMC group. For axial views, $z = -4$; for sagittal views, $x = -12$ (^{18}F-FDG) or $x = -4$ (^{11}C-DED). CTR = control; SPM8 = statistical parametric mapping.

tracer retention in the ADAD carrier and non-carrier groups.

The longitudinal progression of ^{11}C-PiB retention in ADAD carriers demonstrated a significant linear increase in every region of interest except the thalamus, hippocampus and parahippocampus (Table 2 and Fig. 3). The point of separation between the 95% confidence bands of the linear fits for carriers versus non-carriers was used as a conservative estimate of the time point after which the ^{11}C-PiB retention in carriers started to diverge from that in non-carriers. The earliest occurrence of this was at estimated years to symptom onset ≈ -17 years in the putamen and ≈ -15 years in the caudate nucleus, anterior and

posterior cingulate cortices, closely followed temporally at an estimated years to symptom onset ≈ -14 years in the frontal cortex and subsequently other cortical regions. The regional rates of increase in ^{11}C-PiB retention ranged from 0.021 [standard error (SE) 0.006] to 0.036 (SE 0.006) SUVR per year, with the steepest increases observed in the posterior and anterior cingulate cortices, and the putamen. Some individuals in the sMC group showed markedly higher ^{11}C-PiB retention than those in the sporadic Alzheimer's disease group, especially in regions such as the striatum (Fig. 3).

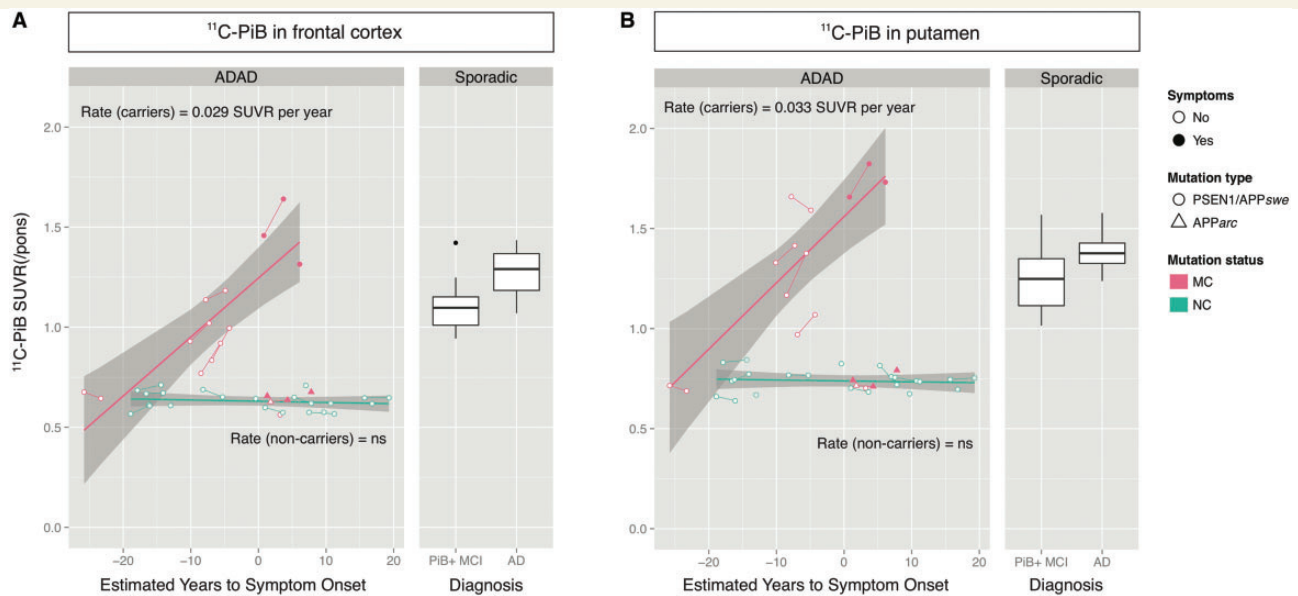The longitudinal change in ^{11}C-DED binding in mutation carrier and non-carrier groups showed more

Figure 3 Time course of baseline and longitudinal regional ^{11}C-PiB retention in ADAD family members. Individual ^{11}C-PiB retention, expressed in SUVR units with reference to the pons, is displayed for (**A**) the frontal cortex and (**B**) the putamen. Symbols: pMC = open red circles (except for APParc carriers = open red triangles); sMC = filled red circles (except for APParc carriers = filled red triangles); non-carrier = open green symbols. Solid lines indicate the regression lines corresponding to the time evolution for mutation carriers (red) and non-carriers (green), obtained from the linear mixed-effects model, along with their confidence bands displayed in grey; the rate of change (SUVR per year) from the model is indicated in each region. Notched boxplots in the right panels show median uptake values in the sporadic PiB + MCI and sporadic Alzheimer's disease patient groups. AD = Alzheimer's disease; MC = mutation carrier; NC = non-carrier; PSEN = presenilin mutation.

intersubject variability than seen with ^{11}C-PiB (Fig. 4). The LMMs showed that ^{11}C-DED binding in ADAD carriers steadily declined with disease progression (estimated years to symptom onset), displaying the highest values in the pMC group from the earliest time before symptom onset. The ^{11}C-DED decline rates in ADAD carriers were significant in every region of interest except the frontal, occipital and the hippocampus regions, with the steepest decline rates reaching −0.030 (SE 0.005) per year in the caudate nucleus and −0.022 (SE 0.007) per year in the thalamus. Most of the individuals in the sMC group showed lower ^{11}C-DED binding than in the sporadic Alzheimer's disease group at baseline (Fig. 4).

The longitudinal ^{18}F-FDG uptake showed significant linear decreases with estimated years to symptom onset in ADAD carriers in all regions of interest except in the parahippocampus (Table 2 and Fig. 5), and significant linear decreases in the non-carrier group in the frontal cortex and caudate nucleus. ^{18}F-FDG uptake in carriers started to diverge from that in the non-carrier group at estimated years to symptom onset ≈ −7 years in the parietal and temporal regions. The respective separation point in subcortical regions including the caudate nucleus, thalamus and hippocampus was at an estimated years to symptom onset ≈ −2 years. The rates of ^{18}F-FDG decrease in ADAD carriers were most pronounced in the caudate nucleus [−0.022 (SE 0.003) SUVR per

year], the posterior cingulate cortex [−0.017 (SE 0.005) SUVR per year] and the parietal cortex [−0.016 (SE 0.003) SUVR per year]. Some of the sMC participants showed markedly more pronounced hypometabolism than observed in the sporadic Alzheimer's disease group at baseline (Fig. 5).

Longitudinal trajectories of regional ^{11}C-PiB, ^{11}C-DED and ^{18}F-FDG PET retention in sporadic Alzheimer's disease

To assess the temporal evolution of the retention of the PET tracers in the sporadic PiB + MCI group, LMMs were performed in this group with respect to time from MCI clinical diagnosis. The uptake of each tracer in the posterior cingulate cortex is shown as example in Supplementary Fig. 1. Statistically significant rates of increase were found for ^{11}C-PiB retention in the putamen [0.042 (SE 0.008) SUVR per year ($P = 0.004$)], insula [0.039 (SE 0.005) SUVR per year ($P = 0.001$)] and parahippocampus [0.013 (SE 0.004) SUVR per year ($P = 0.027$)]. No significant longitudinal rates of change were found for ^{11}C-DED binding in PiB + MCI patients in any region of interest. Finally, ^{18}F-FDG significantly declined in the anterior cingulate cortex at a rate of −0.025 (SE 0.006) SUVR per year ($P = 0.011$).
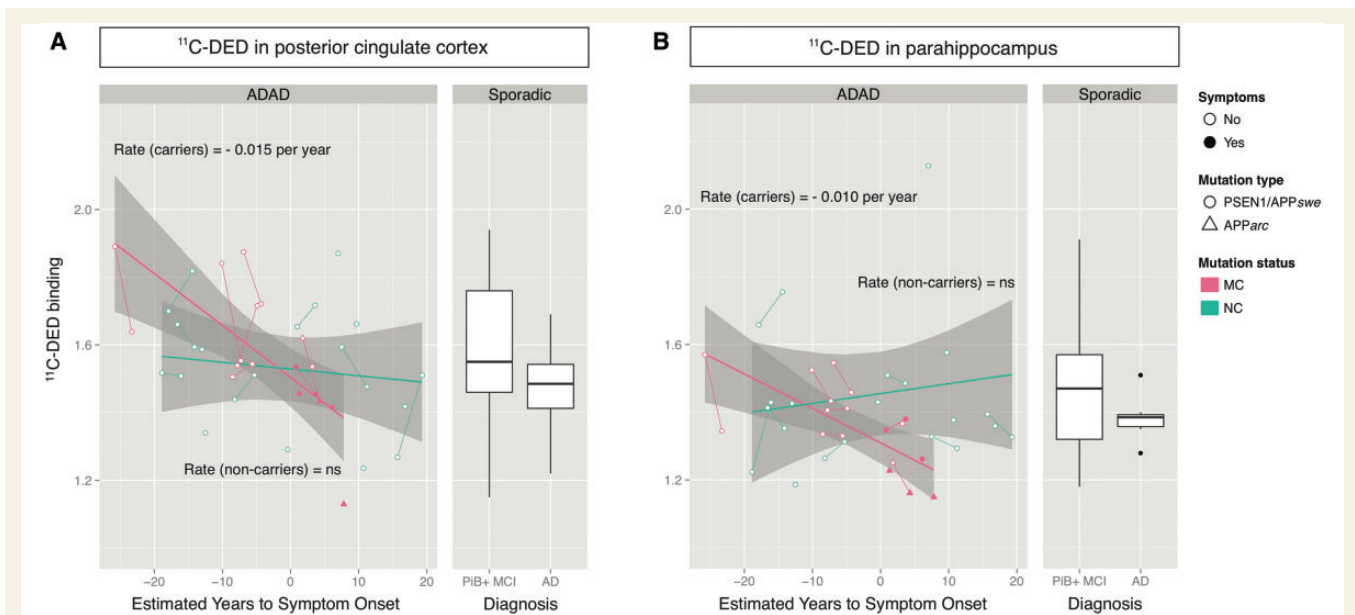
Figure 4 Time course of baseline and longitudinal regional ^{11}C-DED binding in ADAD family members. Individual ^{11}C-DED binding, expressed as the ratio of the Patlak slope (min^{-1}) in the region to that in the cerebellar grey matter (0.01 min^{-1}), is displayed for (**A**) the posterior cingulate cortex and (**B**) the parahippocampus. Symbols: pMC = open red circles (except for APParc carriers = open red triangles); sMC = filled red circles (except for APParc carriers = filled red triangles); non-carrier = open green symbols. Solid lines indicate the regression lines corresponding to the time evolution for mutation carriers (red) and non-carriers (green), obtained from the linear mixed-effects model, along with their confidence bands which are displayed in grey; the rate of change (per year) from the model is indicated in each region. Notched boxplots in the right panels show median uptake values in the sporadic PiB + MCI and sporadic Alzheimer's disease patient groups. AD = Alzheimer's disease; MC = mutation carrier; NC = non-carrier; PSEN = presenilin mutation.
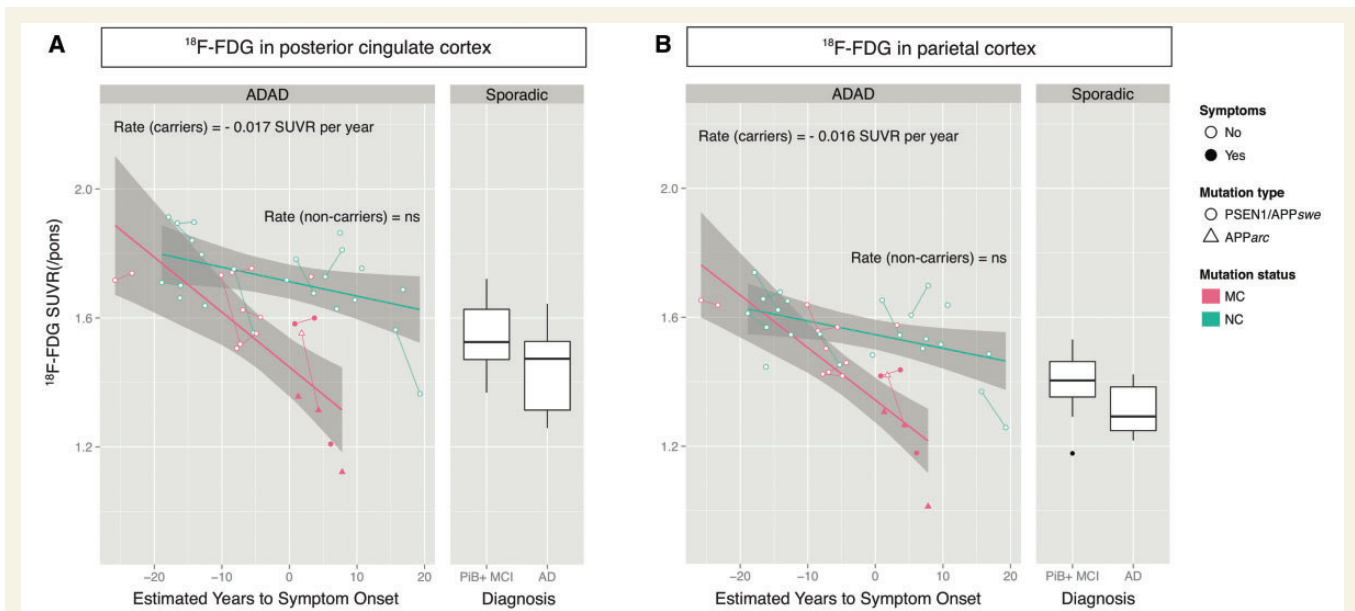

Figure 5 Time course of baseline and longitudinal regional ^{18}F-FDG uptake in ADAD family members. Individual ^{18}F-FDG uptake, expressed in SUVR units with reference to the pons, is displayed for (**A**) the posterior cingulate cortex and (**B**) the parietal cortex. Symbols: pMC = open red circles (except for APParc carriers = open red triangles); sMC = filled red circles (except for APParc carriers = filled red triangles); non-carrier = open green symbols. Solid lines indicate the regression lines corresponding to the time evolution for mutation carriers (red) and non-carriers (green), obtained from the linear mixed-effects model, along with their confidence bands which are displayed in grey; the rate of change (SUVR per year) from the model is indicated in each region. Notched boxplots in the right panels show median uptake values in the sporadic PiB + MCI and sporadic Alzheimer's disease patient groups. AD = Alzheimer's disease; MC = mutation carrier; NC = non-carrier; PSEN = presenilin mutation.

Table 2 Modelling the rates of change of the PET tracers

	¹¹C-PiB, carriers Rate of change (SUVR/year)	¹¹C-DED, carriers Rate of change (/year)	¹⁸F-FDG, carriers Rate of change (SUVR/year)	¹⁸F-FDG, non-carriers Rate of change (SUVR/year)
Cortical regions				
Frontal cortex	**0.029 ± 0.006** (P = 0.005)	ns	**−0.014 ± 0.003** (P = 0.003)	−0.005 ± 0.002 (P = 0.050)
Parietal cortex	**0.029 ± 0.006** (P = 0.004)	−0.008 ± 0.002 (P = 0.014)	**−0.016 ± 0.003** (P = 0.003)	ns
Temporal cortex	**0.027 ± 0.006** (P = 0.006)	−0.007 ± 0.002 (P = 0.010)	**−0.011 ± 0.003** (P = 0.004)	ns
Occipital cortex	**0.021 ± 0.006** (P = 0.022)	ns	**−0.010 ± 0.003** (P = 0.013)	ns
Anterior cingulate cortex	**0.034 ± 0.006** (P = 0.002)	−0.011 ± 0.003 (P = 0.012)	−0.009 ± 0.004 (P = 0.050)	ns
Posterior cingulate cortex	**0.036 ± 0.006** (P = 0.006)	−0.015 ± 0.004 (P = 0.013)	**−0.017 ± 0.005** (P = 0.010)	ns
Insular cortex	**0.026 ± 0.006** (P = 0.006)	−0.012 ± 0.002 (P = 0.002)	**−0.009 ± 0.003** (P = 0.011)	ns
Parahippocampus	ns	−0.010 ± 0.003 (P = 0.016)	ns	ns
Subcortical regions				
Caudate nucleus	**0.025 ± 0.005** (P = 0.005)	**−0.030 ± 0.005** (P = 0.001)	**−0.022 ± 0.003** (P = 0.001)	−0.010 ± 0.003 (P = 0.010)
Putamen	**0.033 ± 0.008** (P = 0.007)	−0.016 ± 0.003 (P = 0.003)	−0.012 ± 0.004 (P = 0.020)	ns
Thalamus	ns	−0.022 ± 0.007 (P = 0.017)	**−0.014 ± 0.002** (P = 0.001)	ns
Hippocampus	ns	ns	**−0.010 ± 0.003** (P = 0.014)	ns

Longitudinal rates of change of PET tracer retention were obtained using a linear mixed-effects model as implemented in the non-linear mixed-effects package in R, including baseline and follow-up data for ¹¹C-PiB, ¹¹C-DED and ¹⁸F-FDG in each region of interest with respect to the estimated number of years to symptom onset. The table includes all significant rates of change ± SE and the corresponding P-values in brackets; the values for the rates of change ± SE are indicated in bold when they remain significant after correction for multiple regional comparisons.
ns = not significant at a threshold of P = 0.05.

Discussion

In this study, we performed a longitudinal follow-up, over a mean period of 2.8 ± 0.6 years, of the regional distribution of brain astrocytosis, amyloid-β plaque deposition and glucose metabolism in patients with ADAD compared to those with sporadic Alzheimer's disease. Previous longitudinal PET imaging studies in ADAD (Benzinger et al., 2013; Yau et al., 2015) reported amyloid-β plaque deposition as the earliest neuropathological change observed in vivo, thus supporting the amyloid cascade hypothesis (Hardy and Higgins, 1992). In this study, we showed evidence of very early astrocyte activation in presymptomatic stages of ADAD, observed at least as early as amyloid-β plaques started to accumulate. The presymptomatic group demonstrated high levels of astrocytosis in comparison with both the Control group and the sporadic symptomatic groups. Overall, initially elevated then declining astrocytosis, increasing amyloid-β plaque deposition, and decreasing glucose metabolism characterized the disease evolution as modelled by ADAD. The time courses of amyloid-β plaque deposition and glucose

metabolism in sporadic patients were overall comparable to those in ADAD participants. While astrocytosis was elevated in sporadic PiB+ MCI patients compared to the Control group and the Alzheimer's disease group, confirming previously reported results (Carter et al., 2012), the longitudinal evolution in this group did not show a significant rate of change.

We observed high fibrillar amyloid-β plaque deposition in the putamen of ADAD carriers as early as 17 years before expected symptom onset, closely followed by the caudate nucleus and other cortical regions. The observed early striatal ¹¹C-PiB retention in the pMC group confirmed our cross-sectional findings comparing pMC with the Control group, and is consistent with previous reports (Klunk et al., 2007; Koivunen et al., 2008; Villemagne et al., 2009; Benzinger et al., 2013). This early striatal amyloid-β plaque deposition in ADAD is also consistent with the observed higher binding of amyloid-β plaque tracers ³H-PiB and ³H-AZD2184 in post-mortem striatal ADAD compared to sporadic Alzheimer's disease brain tissue (Ni, 2015) and provides evidence of pathological

differences between ADAD and sporadic Alzheimer's disease (Shinohara et al., 2014), possibly related to aberrant APP processing caused by the mutation (Potter et al., 2013; Ringman et al., 2014).

Our longitudinal ^{11}C-PiB retention results are also consistent with longitudinal PET imaging in an ADAD cohort (Benzinger et al., 2013) and sporadic populations (Villemagne et al., 2013), both studies showing fibrillar amyloid-β plaque deposition starting from around 15 to 20 years before symptom onset. The results are in contrast with a recent longitudinal PET imaging study in an ADAD cohort, which showed ^{11}C-PiB retention starting 7.5 years before expected symptom onset (Yau et al., 2015); the different timing of initial amyloid-β plaque deposition among studies could be due to differences in mutation types, or to methodological discrepancies regarding definition of symptoms or of age at symptom onset.

Our study allowed obtaining regional rates of change of PET tracer retention. The regions of early ^{11}C-PiB retention in ADAD carriers (including the putamen and the anterior/posterior cingulate cortices) were also those showing the maximum rates of ^{11}C-PiB increase. Consistent with the observed rates of increased ^{11}C-PiB retention in ADAD, the sporadic PiB + MCI group showed similar rates in the putamen and insula. No significant rates of ^{11}C-PiB increase were measured in cortical regions in the sporadic PiB + MCI group, probably because of the limited time span investigated, which was restricted to symptomatic stages, as well as a possible plateau effect on the amyloid-β plaque load, as has been reported in late stages of Alzheimer's disease (Jack and Holtzman, 2013).

The cross-sectional and longitudinal results on ^{11}C-DED binding in ADAD participants in our study have revealed two main findings: an elevated ^{11}C-DED binding in pMC, and diverging temporal patterns of steady ^{11}C-DED decline concomitant with increasing ^{11}C-PiB retention. It is plausible that the initial high ^{11}C-DED binding reflects MAOB elevation in the presence of soluble amyloid-β forms. Several studies have shown that the presence of amyloid-β peptides results in upregulation of gene and protein expression in astrocytes (Mulder et al., 2012; Thal, 2012), including elevated MAOB expression in cultured rat astrocytes (Song et al., 2000). Recent studies have supported the hypothesis that astrocytes have a beneficial role contributing to amyloid-β clearance (Furman et al., 2012), but also that excess amyloid-β can lead to oxidative stress and damage, and as a consequence to reduced astrocyte functionality, leading to reactive changes and decreased neuronal support, and thereby contributing to neurodegeneration (Allaman et al., 2010; Mulder et al., 2012; Thal, 2012). Decreasing MAOB expression in astrocytes with the progression of the disease may be an indication of a reduction in a certain type of astrocyte activation or functionality, a change of astrocyte activation phenotype, or possibly 'astrodegeneration' and astrocyte cell loss itself, as has been reported towards the late stages of Alzheimer's disease

(Smale et al., 1995; Gulyás et al., 2011; Rodriguez-Arellano et al., 2015).

Interestingly, MRI studies in presymptomatic ADAD carriers have shown unexpected early grey matter changes (Fortea et al., 2010; Ryan and Fox, 2013; Ryan et al., 2013; Quiroz et al., 2015; Sala-Llonch et al., 2015), and hypermetabolism preceding hypometabolism (Benzinger et al., 2013), which were interpreted as possibly reflecting glial and neuroinflammatory processes. In our study, although with statistical power limitations, the voxel-wise analyses of pMC data suggested that local astrocytosis could already be high very early, in the presymptomatic stages, when local fibrillar amyloid-β plaque deposition increases. Our longitudinal investigation supports previous cross-sectional findings of presymptomatic astrocytosis from multivariate analysis performed in a subset of participants (Schöll et al., 2015). Similar time courses of astrocytosis and amyloid-β plaque deposition have been observed by in vivo PET imaging in an APPswe mouse model (Rodriguez-Vieitez et al., 2015).

The pMC group had greater ^{11}C-DED binding in the anterior cingulate cortex and thalamus than sporadic PiB + MCI patients. These two regions might represent the sites of earliest astrocyte activation in the course of ADAD. Future research on earlier stages in at-risk sporadic cohorts would help elucidate whether sporadic Alzheimer's disease has a similar regional pattern of early brain astrocytosis to that observed in ADAD. The longitudinal investigation of ^{11}C-DED binding in PiB + MCI patients did not reveal a significant rate of change with time. Possible explanations for this finding include the heterogeneity of disease stage in MCI patients, the shorter time span investigated in the sporadic patients compared to the ADAD participants, or a possibly different progression of astrocyte activation in the sporadic compared to the autosomal dominant forms.

Glucose metabolism declined significantly in both carriers and non-carriers. The observed metabolic decline in the frontal cortex and caudate nucleus in non-carriers is in agreement with findings in healthy ageing adults (Yoshizawa et al., 2014). The decline in glucose metabolism in ADAD carriers started to deviate significantly from that in non-carriers at estimated years to symptom onset ≈ −7 years in the parieto-temporal cortex, which is typically hypometabolic in sporadic Alzheimer's disease (La Joie et al., 2012), about a decade after the start of amyloid-β plaque deposition. The pMC group showed preserved metabolism in most subcortical regions including the putamen, which, however, showed amyloid-β plaque deposition. Our results are largely consistent with previous studies where hypometabolism in ADAD carriers was first observed from ≈−10 to −5 estimated years to symptom onset in cortical regions, while subcortical metabolism was preserved in the presymptomatic stages except in the hippocampus (Benzinger et al., 2013). In contrast, a recent longitudinal study in ADAD reported that the earliest hypometabolism was observed only in temporal coincidence with the onset of symptoms (Yau et al., 2015),

which could be partly due to methodological differences. Some of the sMC patients in our study showed more pronounced hypometabolism than seen in sporadic Alzheimer's disease (Fig. 5), confirming previous findings (Schöll et al., 2011b). In our sporadic PiB+ MCI patients, we observed longitudinal decline rates similar to those in ADAD carriers, although in fewer brain regions, probably because of the relatively shorter time span investigated.

Different mutations result in variations in pathology and disease progression (Shinohara et al., 2014). One limitation of our study was that all the mutation types were combined, except for the Arctic carriers, who were excluded from the ^{11}C-PiB PET group analyses. In addition, while the progression of PET tracer retention in pMC participants is probably different from that in sMC patients, the limited number of sMC patients did not allow for statistical comparisons, and LMMs were applied to the combination of pMC and sMC data. Therefore, the predictions of the LMMs should be interpreted with some caution. However, the observed low values of ^{18}F-FDG uptake and ^{11}C-DED binding in individual sMC patients suggests a somewhat more aggressive neurodegeneration pattern in ADAD than in sporadic Alzheimer's disease. For future research, additional follow-up examinations per patient will allow more suitable non-linear modelling of the neuropathological time courses with disease progression.

In conclusion, the longitudinal examination of ADAD and sporadic Alzheimer's disease participants with an average follow-up time of 2.8 ± 0.6 years showed the diverging regional and time courses of Alzheimer's disease-related biomarkers as measured by PET imaging. Prominent initial and then declining astrocytosis, increasing fibrillar amyloid-β plaque pathology and decreasing glucose metabolism characterized ADAD evolution. Similar time courses of amyloid-β plaque deposition and glucose metabolism were observed in patients with sporadic Alzheimer's disease and ADAD. Although higher levels of astrocytosis were observed in the presymptomatic ADAD group than in the sporadic PiB+ MCI and Alzheimer's disease groups, astrocytosis was still observable early on in the sporadic forms of the disease. Studies of larger cohorts would be useful for further investigating the earlier stages to elucidate whether the presymptomatic astrocytosis observed in ADAD is also found in sporadic Alzheimer's disease. Future longitudinal *in vivo* studies including, in addition to astrocytosis, also imaging of other neuroinflammatory components and tau deposition in brain would be useful for further advancement of imaging biomarkers and contribute to development of disease-modifying therapies.

Supplementary material

Supplementary material is available at *Brain* online.

References

Allaman I, Gavillet M, Bélanger M, Laroche T, Viertl D, Lashuel HA, et al. Amyloid-beta aggregates cause alterations of astrocytic metabolic phenotype: impact on neuronal viability. J Neurosci 2010; 30: 3326–38.

Anderson MA, Ao Y, Sofroniew MV. Heterogeneity of reactive astrocytes. Neurosci Lett 2014; 565: 23–9.

Barres BA. The mystery and magic of glia: a perspective on their roles in health and disease. Neuron 2008; 60: 430–40.

Bateman RJ, Aisen PS, De Strooper B, Fox NC, Lemere CA, Ringman JM, et al. Autosomal-dominant Alzheimer's disease: a review and proposal for the prevention of Alzheimer's disease. Alzheimers Res Ther 2011; 3: 1.

Bateman RJ, Xiong C, Benzinger TL, Fagan AM, Goate A, Fox NC, et al. Clinical and biomarker changes in dominantly inherited Alzheimer's disease. N Engl J Med 2012; 367: 795–804.

Benjamini Y, Hochberg Y. Controlling the false discovery rate—a practical and powerful approach to multiple testing. J Roy Stat Soc B Met 1995; 57: 289–300.

Benzinger TL, Blazey T, Jack CR, Jr, Koeppe RA, Su Y, Xiong C, et al. Regional variability of imaging biomarkers in autosomal dominant Alzheimer's disease. Proc Natl Acad Sci USA 2013; 110: E4502–9.

Braak H, Braak E. Neuropathological stageing of Alzheimer-related changes. Acta Neuropathol 1991; 82: 239–59.

Carter SF, Schöll M, Almkvist O, Wall A, Engler H, Långström B, et al. Evidence for astrocytosis in prodromal Alzheimer disease provided by 11C-deuterium-L-deprenyl: a multitracer PET paradigm combining 11C-Pittsburgh compound B and 18F-FDG. J Nucl Med 2012; 53: 37–46.

Chételat G. Alzheimer disease: abeta-independent processes-rethinking preclinical AD. Nat Rev Neurol 2013; 9: 123–4.

Choo IH, Carter SF, Schöll ML, Nordberg A. Astrocytosis measured by (11)C-deprenyl PET correlates with decrease in gray matter density in the parahippocampus of prodromal Alzheimer's patients. Eur J Nucl Med Mol Imaging 2014; 41: 2120–6.

Dubois B, Feldman HH, Jacova C, Hampel H, Molinuevo JL, Blennow K, et al. Advancing research diagnostic criteria for Alzheimer's disease: the IWG-2 criteria. Lancet Neurol 2014; 13: 614–29.

Dunn OJ. Multiple comparisons using rank sums. Technometrics 1964; 6: 241–52.

Ekblom J, Jossan SS, Bergström M, Oreland L, Walum E, Aquilonius SM. Monoamine oxidase-B in astrocytes. Glia 1993; 8: 122–32.

Fleisher AS. The value of biomarker comparisons between autosomal dominant and late-onset Alzheimer disease. JAMA Neurol 2014; 71: 1087–8.

Fleisher AS, Chen K, Quiroz YT, Jakimovich LJ, Gomez MG, Langois CM, et al. Florbetapir PET analysis of amyloid-beta deposition in the presenilin 1 E280A autosomal dominant Alzheimer's disease kindred: a cross-sectional study. Lancet Neurol 2012; 11: 1057–65.

Fleisher AS, Chen K, Quiroz YT, Jakimovich LJ, Gutierrez Gomez M, Langois CM, et al. Associations between biomarkers and age in the presenilin 1 E280A autosomal dominant Alzheimer disease kindred: a cross-sectional study. JAMA Neurol 2015; 72: 316–24.

Fortea J, Sala-Llonch R, Bartres-Faz D, Bosch B, Llado A, Bargallo N, et al. Increased cortical thickness and caudate volume precede atrophy in PSEN1 mutation carriers. J Alzheimers Dis 2010; 22: 909–22.

Fowler JS, MacGregor RR, Wolf AP, Arnett CD, Dewey SL, Schlyer D, et al. Mapping human brain monoamine oxidase A and B with 11C-labeled suicide inactivators and PET. Science 1987; 235: 481–5.

Fowler JS, Logan J, Volkow ND, Wang G-J. Translational neuroimaging: positron emission tomography studies of monoamine oxidase. Mol Imaging Biol 2005; 7: 377–87.

Fuller S, Munch G, Steele M. Activated astrocytes: a therapeutic target in Alzheimer's disease?. Expert Rev Neurother 2009; 9: 1585–94.

Furman JL, Sama DM, Gant JC, Beckett TL, Murphy MP, Bachstetter AD, et al. Targeting astrocytes ameliorates neurologic changes in a mouse model of Alzheimer's disease. J Neurosci 2012; 32: 16129–40.

Gulyás B, Pavlova E, Kása P, Gulya K, Bakota L, Várszegi S, et al. Activated MAO-B in the brain of Alzheimer patients, demonstrated by [11C]-L-deprenyl using whole hemisphere autoradiography. Neurochem Int 2011; 58: 60–8.

Hammers A, Allom R, Koepp MJ, Free SL, Myers R, Lemieux L, et al. Three-dimensional maximum probability atlas of the human brain, with particular reference to the temporal lobe. Hum Brain Mapp 2003; 19: 224–47.

Hardy JA, Higgins GA. Alzheimer's disease: the amyloid cascade hypothesis. Science 1992; 256: 184–5.

Heneka MT, Carson MJ, Khoury JE, Landreth GE, Brosseron F, Feinstein DL, et al. Neuroinflammation in Alzheimer's disease. Lancet Neurol 2015a; 14: 388–405.

Heneka MT, Golenbock DT, Latz E. Innate immunity in Alzheimer's disease. Nat Immunol 2015b; 16: 229–36.

Holtzman DM, Morris JC, Goate AM. Alzheimer's disease: the challenge of the second century. Sci Transl Med 2011; 3: 77sr1.

Hyman BT. Amyloid-dependent and amyloid-independent stages of Alzheimer disease. Arch Neurol 2011; 68: 1062–4.

Jack CR, Jr, Holtzman DM. Biomarker modeling of Alzheimer's disease. Neuron 2013; 80: 1347–58.

Jacobs AH, Tavitian B, Consortium I. Noninvasive molecular imaging of neuroinflammation. J Cereb Blood Flow Metab 2012; 32: 1393–415.

Johansson A, Engler H, Blomquist G, Scott B, Wall A, Aquilonius SM, et al. Evidence for astrocytosis in ALS demonstrated by [11C](L)-deprenyl-D2 PET. J Neurol Sci 2007; 255: 17–22.

Kadir A, Marutle A, Gonzalez D, Schöll M, Almkvist O, Mousavi M, et al. Positron emission tomography imaging and clinical progression in relation to molecular pathology in the first Pittsburgh Compound B positron emission tomography patient with Alzheimer's disease. Brain 2011; 134(Pt 1): 301–17.

Keller L, Welander H, Chiang HH, Tjernberg LO, Nennesmo I, Wallin AK, et al. The PSEN1 I143T mutation in a Swedish family with Alzheimer's disease: clinical report and quantification of Abeta in different brain regions. Eur J Hum Genet 2010; 18: 1202–8.

Klunk WE, Price JC, Mathis CA, Tsopelas ND, Lopresti BJ, Ziolko SK, et al. Amyloid deposition begins in the striatum of presenilin-1 mutation carriers from two unrelated pedigrees. J Neurosci 2007; 27: 6174–84.

Koivunen J, Verkkoniemi A, Aalto S, Paetau A, Ahonen JP, Viitanen M, et al. PET amyloid ligand [11C]PIB uptake shows predominantly striatal increase in variant Alzheimer's disease. Brain 2008; 131(Pt 7): 1845–53.

La Joie R, Perrotin A, Barre L, Hommet C, Mezenge F, Ibazizene M, et al. Region-specific hierarchy between atrophy, hypometabolism, and beta-amyloid (Abeta) load in Alzheimer's disease dementia. J Neurosci 2012; 32: 16265–73.

Marutle A, Gillberg PG, Bergfors A, Yu W, Ni R, Nennesmo I, et al. 3H-Deprenyl and 3H-PIB autoradiography show different laminar distributions of astroglia and fibrillar beta-amyloid in Alzheimer brain. J Neuroinflammation 2013; 10: 90.

McKhann G, Drachman D, Folstein M, Katzman R, Price D, Stadlan EM. Clinical diagnosis of Alzheimer's disease: report of the NINCDS-ADRDA Work Group under the auspices of department of health and human services task force on Alzheimer's disease. Neurology 1984; 34: 939–44.

Miller G. Neuroscience. The dark side of glia. Science 2005; 308: 778–81.

Minoshima S, Frey KA, Foster NL, Kuhl DE. Preserved pontine glucose metabolism in Alzheimer disease: a reference region for functional brain image (PET) analysis. J Comput Assist Tomogr 1995; 19: 541–7.

Mulder SD, Veerhuis R, Blankenstein MA, Nielsen HM. The effect of amyloid associated proteins on the expression of genes involved in amyloid-beta clearance by adult human astrocytes. Exp Neurol 2012; 233: 373–9.

Ni R. Multiple amyloid binding sites in Alzheimer brain and their interaction with synaptic and inflammatory mechanisms. Doctoral Thesis. Karolinska Institutet, Sweden; 2015. ISBN: 978-91-7549-873-7.

Nordberg A, Carter SF, Rinne J, Drzezga A, Brooks DJ, Vandenberghe R, et al. A European multicentre PET study of fibrillar amyloid in Alzheimer's disease. Eur J Nucl Med Mol Imaging 2013; 40: 104–14.

Oberheim NA, Goldman SA, Nedergaard M. Heterogeneity of astrocytic form and function. Methods Mol Biol 2012; 814: 23–45.

Petersen RC. Mild cognitive impairment as a diagnostic entity. J Intern Med 2004; 256: 183–94.

Potter R, Patterson BW, Elbert DL, Ovod V, Kasten T, Sigurdson W, et al. Increased *in vivo* amyloid-beta42 production, exchange, and loss in presenilin mutation carriers. Sci Transl Med 2013; 5: 189ra77.

Quiroz YT, Schultz AP, Chen K, Protas HD, Brickhouse M, Fleisher AS, et al. Brain imaging and blood biomarker abnormalities in children with autosomal dominant Alzheimer disease: a cross-sectional study. JAMA Neurol 2015; 72: 912–9.

Ringman JM, Goate A, Masters CL, Cairns NJ, Danek A, Graff-Radford N, et al. Genetic heterogeneity in Alzheimer disease and implications for treatment strategies. Curr Neurol Neurosci Rep 2014; 14: 499.

Rodriguez-Arellano JJ, Parpura V, Zorec R, Verkhratsky A. Astrocytes in physiological aging and Alzheimer's disease. Neuroscience 2015; http://dx.doi.org/10.1016/j.neuroscience.2015.01.007.

Rodriguez-Vieitez E, Ni R, Gulyás B, Tóth M, Häggkvist J, Halldin C, et al. Astrocytosis precedes amyloid plaque deposition in Alzheimer APPswe transgenic mouse brain: a correlative positron emission tomography and in vitro imaging study. Eur J Nucl Med Mol Imaging 2015; 42: 1119–32.

Ryan NS, Fox NC. Reply: implications of presymptomatic change in thalamus and caudate in Alzheimer's disease. Brain 2013; 136(Pt 11): e259.

Ryan NS, Keihaninejad S, Shakespeare TJ, Lehmann M, Crutch SJ, Malone IB, et al. Magnetic resonance imaging evidence for presymptomatic change in thalamus and caudate in familial Alzheimer's disease. Brain 2013; 136(Pt 5): 1399–414.

Ryman DC, Acosta-Baena N, Aisen PS, Bird T, Danek A, Fox NC, et al. Symptom onset in autosomal dominant Alzheimer disease: a systematic review and meta-analysis. Neurology 2014; 83: 253–60.

Sala-Llonch R, Lladó A, Fortea J, Bosch B, Antonell A, Balasa M, et al. Evolving brain structural changes in PSEN1 mutation carriers. Neurobiol Aging 2015; 36: 1261–70.

Santillo AF, Gambini JP, Lannfelt L, Långström B, Ulla-Marja L, Kilander L, et al. In vivo imaging of astrocytosis in Alzheimer's disease: an C-11-L-deuteriodeprenyl and PIB PET study. Eur J Nucl Med Mol Imaging 2011; 38: 2202–8.

Saura J, Luque JM, Cesura AM, Da Prada M, Chan-Palay V, Huber G, et al. Increased monoamine oxidase B activity in plaque-associated astrocytes of Alzheimer brains revealed by quantitative enzyme radioautography. Neuroscience 1994; 62: 15–30.

Schöll M, Almkvist O, Axelman K, Stefanova E, Wall A, Westman E, et al. Glucose metabolism and PIB binding in carriers of a His163Tyr presenilin 1 mutation. Neurobiol Aging 2011a; 32: 1388–99.

Schöll M, Almkvist O, Bogdanovic N, Wall A, Långström B, Viitanen M, et al. Time course of glucose metabolism in relation to cognitive performance and postmortem neuropathology in Met146Val PSEN1 mutation carriers. J Alzheimers Dis 2011b; 24: 495–506.

Schöll M, Wall A, Thordardottir S, Ferreira D, Bogdanovic N, Långström B, et al. Low PiB PET retention in presence of pathologic CSF biomarkers in Arctic APP mutation carriers. Neurology 2012; 79: 229–36.

Schöll M, Carter SF, Westman E, Rodriguez-Vieitez E, Almkvist O, Thordardottir S, et al. Early astrocytosis in autosomal dominant Alzheimer's disease measured in vivo by multi-tracer positron emission tomography. Sci Rep 2015; 5: 16404.

Shinohara M, Fujioka S, Murray ME, Wojtas A, Baker M, Rovelet-Lecrux A, et al. Regional distribution of synaptic markers and APP correlate with distinct clinicopathological features in sporadic and familial Alzheimer's disease. Brain 2014; 137(Pt 5): 1533–49.

Smale G, Nichols NR, Brady DR, Finch CE, Horton WE, Jr. Evidence for apoptotic cell death in Alzheimer's disease. Exp Neurol 1995; 133: 225–30.

Song W, Zhou LJ, Zheng SX, Zhu XZ. Amyloid-beta 25–35 peptide induces expression of monoamine oxidase B in cultured rat astrocytes. Acta Pharmacol Sin 2000; 21: 557–63.

Thal DR. The role of astrocytes in amyloid beta-protein toxicity and clearance. Exp Neurol 2012; 236: 1–5.

Thomas JB, Brier MR, Bateman RJ, Snyder AZ, Benzinger TL, Xiong C, et al. Functional connectivity in autosomal dominant and late-onset Alzheimer disease. JAMA Neurol 2014; 71: 1111–22.

Thordardottir S, Ståhlbom AK, Ferreira D, Almkvist O, Westman E, Zetterberg H, et al. Preclinical cerebrospinal fluid and volumetric magnetic resonance imaging biomarkers in Swedish familial Alzheimer's disease. J Alzheimers Dis 2014; 43: 1393–402.

Turkheimer FE, Smith CB, Schmidt K. Estimation of the number of "true" null hypotheses in multivariate analysis of neuroimaging data. Neuroimage 2001; 13: 920–30.

Varley J, Brooks DJ, Edison P. Imaging neuroinflammation in Alzheimer's and other dementias: recent advances and future directions. Alzheimers Dement 2015; 11: 1110–20.

Verkhratsky A, Marutle A, Rodriguez-Arellano JJ, Nordberg A. Glial asthenia and functional paralysis: a new perspective on neurodegeneration and Alzheimer's disease. Neuroscientist 2015; 21: 552–68.

Villemagne VL, Ataka S, Mizuno T, Brooks WS, Wada Y, Kondo M, et al. High striatal amyloid beta-peptide deposition across different autosomal Alzheimer disease mutation types. Arch Neurol 2009; 66: 1537–44.

Villemagne VL, Burnham S, Bourgeat P, Brown B, Ellis KA, Salvado O, et al. Amyloid beta deposition, neurodegeneration, and cognitive decline in sporadic Alzheimer's disease: a prospective cohort study. Lancet Neurol 2013; 12: 357–67.

Yau WW, Tudorascu DL, McDade EM, Ikonomovic S, James JA, Minhas D, et al. Longitudinal assessment of neuroimaging and clinical markers in autosomal dominant Alzheimer's disease: a prospective cohort study. Lancet Neurol 2015; 14: 804–13.

Yoshizawa H, Gazes Y, Stern Y, Miyata Y, Uchiyama S. Characterizing the normative profile of 18F-FDG PET brain imaging: sex difference, aging effect, and cognitive reserve. Psychiatry Res 2014; 221: 78–85.

Yu WF, Guan ZZ, Bogdanovic N, Nordberg A. High selective expression of alpha7 nicotinic receptors on astrocytes in the brains of patients with sporadic Alzheimer's disease and patients carrying Swedish APP 670/671 mutation: a possible association with neuritic plaques. Exp Neurol 2005; 192: 215–25.

Zhang Y, Barres BA. Astrocyte heterogeneity: an underappreciated topic in neurobiology. Curr Opin Neurobiol 2010; 20: 588–94.

Zimmer ER, Leuzy A, Benedet AL, Breitner J, Gauthier S, Rosa-Neto P. Tracking neuroinflammation in Alzheimer's disease: the role of positron emission tomography imaging. J Neuroinflammation 2014; 11: 120.

Zlokovic BV. Neurovascular pathways to neurodegeneration in Alzheimer's disease and other disorders. Nat Rev Neurosci 2011; 12: 723–38.